Chemical Science

ROYAL SOCIETY OF CHEMISTRY

EDGE ARTICLE

View Article Online
View Journal | View Issue

Cite this: *Chem. Sci.*, 2024, **15**, 13688

All publication charges for this article have been paid for by the Royal Society of Chemistry

Harnessing a bis-electrophilic boronic acid lynchpin for azaborolo thiazolidine (ABT) grafting in cyclic peptides†

Basab Kanti Das,‡ Arnab Chowdhury, ‡ Saurav Chatterjee, Nitesh Mani Tripathi, Bibekananda Pati, Soumit Dutta and Anupam Bandyopadhyay *

Received 1st July 2024
Accepted 24th July 2024

DOI: 10.1039/d4sc04348k

rsc.li/chemical-science

Chemical modifications of native peptides have significantly advanced modern drug discovery in recent decades. On this front, the installation of multitasking molecular grafts onto macrocyclic peptides offers numerous opportunities in biomedical applications. Here, we showcase a new class of borono-cyclic peptides featuring an azaborolo thiazolidine (ABT) graft, which can be readily assembled utilizing a bis-electrophilic boronic acid lynchpin while harnessing the inherent reactivity difference (>10^3 M^{-1} s^{-1}) between the N-terminal cysteine and backbone cysteine for rapid and highly regioselective macrocyclization (~1 h) under physiological conditions. The ABT-crosslinked peptides are fairly stable in endogenous environments, but can provide the linear diazaborine peptides *via* treatment with α-nucleophiles. This efficient peptide crosslinking protocol was further extended for regioselective bicyclizations and engineering of α-helical structures. Finally, ABT-grafted peptides were exploited in biorthogonal conjugation, leading to highly effective intracellular delivery of an apoptotic peptide (KLA) in cancer cells. The mechanism of action by which ABT-grafted KLA peptide induces apoptosis was also explored.

Introduction

Peptides provide a unique three-dimensional chemical space between small molecules and large biologics, with enormous potential for drug development.[1] However, as a consequence of their conformational freedom, most linear short peptides suffer from pharmacological liabilities, *viz.* proteolytic degradation, low binding affinity, and low target selectivity. To address these drawbacks, chemical modification and macrocyclization of bioactive peptides have proven advantageous and have emerged as a modern research hotspot for various disciplines.[2] Peptide macrocyclization has enabled extensive chemical spacing, folding, and rigidification of peptide architectures, resulting in improved target binding, proteolytic and metabolic stability, and cell penetration.[3] To date, various peptide macrocyclization methods are documented in the literature, each offering its own unique advantages. These include the formation of thioacetal,[4–6] oxime,[7] imine,[8] and thioether[9,10] linkages, as well as the deployment of click chemistry,[11,12] olefin metathesis,[13,14] and KAHA ligation[15,16] regimens, along with many other approaches.[17] A recent effort by Yudin and Chen's group has shown that the crosslinking of one or more aromatic side chains can achieve highly strained cyclophane-type macrocycles in peptide chains.[18]

Contingent to the progress made in the chemoselective crosslinking of peptide backbones,[19] the regioselective crosslinking of native peptides, especially cysteine-rich peptides, offers multiple opportunities in peptide engineering. For example, Brik's group adopted a *de novo* peptide cyclization strategy, forging two or three disulfide bonds in peptides or proteins in a chemo- and regioselective manner by judiciously utilizing the interplay between the orthogonal *S*-protecting groups on the native cysteine residues.[20,21] Another study applied NHS-activated acrylamide for chemoselective amino-sulfhydryl crosslinking on native peptides.[22] Recent efforts have also been directed towards the bis-electrophilic regioselective crosslinking of the N-terminus to backbone cysteines in phage-displayed peptide libraries.[23–26] Nevertheless, in the context of peptide-based drug discovery, it is imperative to widen the scope of the regioselective crosslinking of cysteine-rich peptides for site-selective, exclusive macrocyclization[27] towards the synthesis of functionally advanced molecular entities.[28–30] Because the regioselective crosslinking of cysteine-rich peptides with bis-electrophiles is relatively less explored, there are ample opportunities to leverage the adjoining of versatile functional

Biomimetic Peptide Engineering Laboratory, Department of Chemistry, Indian Institute of Technology Ropar, Rupnagar, Punjab 140001, India. E-mail: anupamba@iitrpr.ac.in

† Electronic supplementary information (ESI) available. See DOI: https://doi.org/10.1039/d4sc04348k

‡ BKD and AC contributed equally.

handles, such as heterocycles, click handles, covalent probes, and various synthetic scaffolds for wide prospects. For instance, derivatizing a variety of Lugdunin cyclopeptide[31] analogs by the installation of thiazolidine-based molecular entities could lead to a potent antibacterial agent.

In our quest for engineered boronopeptides for biochemical applications,[32–34] it was noted that borono-heterocycles are rarely seen in peptide frameworks and could provide an enormous range of novel biochemical applications. We conceptualized a regioselective peptide crosslinking method *via* the formation of azaborolo thiazolidine (**ABT**) grafts (Fig. 1a), in which the inherent Wulff-boronate[35,36] biorthogonal handle and the thiazolidine[37] moiety could be judiciously utilized to increase the chemical space. For instance, peptide frameworks modulated with heterocycles[38] or boronic acid[39] can facilitate cell penetration. In particular, boronic acid's versatile interaction modules (noncovalent and covalent)[40] could provide diverse attractive prospects using this concept. It is also anticipated that the ABT graft could be released by specific α-nucleophiles to offer a linear peptide displaying diazaborine derivatives, which are of great interest for stimuli-responsive chemistry[41] and the development of antibacterial agents.[42] Towards this end, we now report a highly regioselective peptide macrocyclization using bis-electrophilic iodoacetamide tethered 2-formyl phenylboronic acid (2-FPBA) lynchpins, first through selective and quantitative engagement of the N-terminal cysteine to form azaborolo thiazolidine (**ABT**) grafts, followed by proximity-driven thioalkylation reactions with the

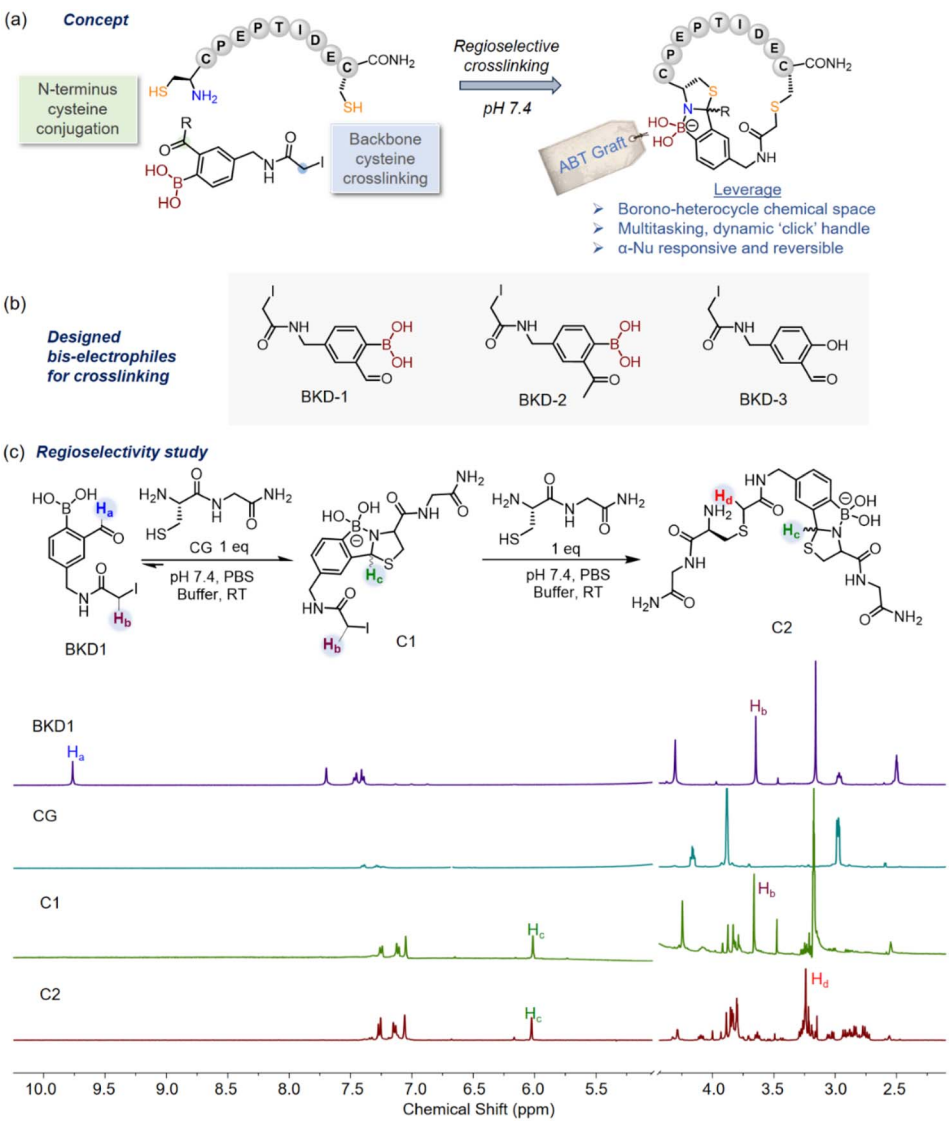

Fig. 1 (a) The concept of regioselective crosslinking at physiological pH, which, judiciously combined with the inherent Wulff-boronate handle and the thiazolidine moiety, can provide advantages in biochemical applications. (b) Chemical structure of the bis-electrophiles used for the investigation of regioselective crosslinking. (c) Scheme of the regioselective sequential reactions between CG and BKD1, in which a precise equivalency between CG and BKD1 was maintained by ^{1}H-NMR titration from a stock solution. The ^{1}H-NMR data clearly demonstrate the tandem reactivity of the bis-electrophile BKD1. The highlighted protons in the scheme correlate with the chemical shift changes in the ^{1}H-NMR data recorded in (1 : 4) D_2O : PBS (7.4).

backbone cysteines. This method further allows the facile construction of bicyclic peptides by establishing an additional disulfide bond in a regioselective manner. Finally, we demonstrate our efforts toward an engineered dual-functional peptide scaffold engaging ABT crosslinking, simultaneously folding a pro-apoptotic peptide into a secondary structure and delivering it into cancer cells by applying dynamic salicylhydroxamic boronate (SHAB)[42] conjugation chemistry.

Results and discussion

Design of regioselective tandem bis-electrophile

The cysteine residue has featured in many chemoselective bioconjugation reactions due to its low interactome abundance and high nucleophilicity under physiological conditions.[43–46] In this work, we envisaged regioselective crosslinking between two different types of cysteine found in native peptides, *i.e.*, N-terminus cysteine and backbone cysteine, deploying bis-electrophilic lynchpins that were strategically functionalized with two kinetically distinctive electrophiles for selective orthogonal reactions (Fig. 1a and b). We combined a 2-FPBA moiety with the classical cysteine alkylating agent iodoacetamide (*e.g.*, BKD1, Fig. 1b, ESI Section IIIa†), leveraging the superior reactivity of N-terminal cysteines with 2-FPBA ($>10^3$ M^{-1} s^{-1})[47] *vis-a-vis* iodoacetamide-mediated *S*-alkylation to ensure orthogonal cross reactivity. The native peptides were expected to first react with BKD-1 preferentially *via* the N-terminus cysteine to form a thermodynamically stable azaborolo thiazolidine (**ABT**) conjugate and subsequently engage in proximity-driven *S*-alkylation with backbone cysteine, leading to macrocyclization. The macrocyclic ABT conjugates could be further edited as a dynamic 'click' handle[42] while benefitting from boronic acid (**BA**) fusion with the thiazolidine heterocycle[37] for diverse biological submissions. As controls, we also prepared two other bis-electrophiles, BKD2 and BKD3, based on 2-acetyl phenylboronic acid (2-APBA) and 2-hydroxy benzaldehyde (2-HB) (Fig. 1b). While 2-APBA is known to combine rapidly with N-terminus cysteine at physiological pH, its ABT conjugate is thermodynamically less stable compared to 2-FPBA.[42] The 2-HB derivatives are also known to produce thiazolidine derivatives with N-terminal cysteine but with sluggish kinetics even at a slightly acidic pH.[47]

The regioselectivity of the designed bis-electrophiles BKD1-3 towards cysteine bioconjugation was probed through ^{1}H-NMR experiments using a cysteine dipeptide (CG) in PBS buffer (pH 7.4) (Fig. 1c). An equimolar mixture of CG and BKD1 (~1 mM each) resulted in a rapid disappearance of the formyl proton at 9.85 ppm with the concomitant appearance of two diastereomeric protons of the ABT conjugate (**C1**) at around 6.0–6.2 ppm. ABT conjugate formation was further confirmed by the upfield shifting of the aromatic protons, accompanied by enhanced splitting. The addition of an extra equivalent of CG to this mixture caused an upfield shift of the side-chain iodoacetamide methylene protons from 3.68 ppm to 3.23 ppm, indicating side-chain *S*-alkylation to form the bis-adduct **C2** (Fig. 1c). On the other hand, the addition of ~1.0 equivalent of CG to BKD2 only caused an upfield shift of the methylene protons of BKD2, indicating the occurrence of the promiscuous *S*-alkylation of the iodoacetamide side chain as the primary reaction (Fig. S1†), perhaps due to the reversible nature of ABT conjugation with the more sterically hindered 2-APBA probe. Furthermore, treatment of salicylaldehyde-derived probe BKD3 with CG only indicated the side-chain *S*-alkylated product with no thiazolidine formation, even with 2.0 equivalents of CG. (Fig. S2†). Based on these findings, the 2-FPBA-derived BKD-1 emerged as the optimum bis-electrophile for our crosslinking purposes.

Investigation of regioselective peptide crosslinking

The crosslinking ability of BKD-1 was examined using the model peptide CIITRPC. After incubation of equimolar concentrations (~100 μM) of BKD-1 and CIITRPC at pH 7.4 for only 30 min, a prominent peak corresponding to the crosslinked peptide P1 appeared in the LC-MS spectrum (Fig. 2a, ESI Section V†), confirming our hypothesis that the 2-FPBA based bis-electrophilic lynchpins were highly effective cysteine crosslinking scaffolds for the regioselective macrocyclization of native peptides. In contrast, as expected, treating BKD-2 with the peptide CIITRPC yielded two major peaks in the LC, indicating the formation of two side-chain cysteine-alkylated products, as confirmed by mass analysis (ESI Fig. S3†). Notably, the crosslinked peptide **P1** generated a mixture of two diastereomers around the thiazolidine heterocycle. The presence of diastereomeric thiazolidines in the natural cyclopeptide lugdunin,[31] an antibiotic, served as an additional impetus to pursue our ABT crosslinking campaign.

Encouraged by the prospects of BKD-1 as an efficient cysteine crosslinking module, we undertook detailed ^{1}H- and ^{11}B-NMR studies of its reaction with CIITRPC in PBS buffer. Upon crosslinking with CIITRPC, BKD-1 exhibited distinct proton chemical shifts due to the formation of the ABT conjugate and *S*-alkylation of the iodoacetamide unit (Fig. 2b), a pattern which is similar to the signature shown by **C2** (*cf.* Fig. 1c). In the ^{11}B-NMR spectrum, the ABT unit in the crosslinked peptide P1 showed a chemical shift at 8.30 ppm (Fig. 2c), indicating the exclusive population of N–B connected heterocycles.[47] BKD1 alone shows a chemical shift at ~30 ppm in an ^{11}B-NMR spectrum (ESI Section VIII and Fig. S7†). To explore the kinetics of the cyclization process, we performed LC-MS analysis of the reaction between CIITRPC and BKD1 (~100 μM each) over time and calculated the half-life (Fig. 2d, ESI Section VI and Fig. S4†). The obtained k value aligns with the proximity-driven *S*-alkylation reaction (first-order kinetics), providing additional support to our hypothesis. The initial **ABT** formation occurred rapidly ($>10^3$ M^{-1} s^{-1})[47] within a few seconds at 100 μM so that the subsequent *S*-alkylation step turned into the rate-determining (RD) step ($t_{1/2}$ ~ 11 min), governing the overall cyclization kinetics. However, the kinetics could differ with varying the length of the peptide sequence.

The veracity of the macrocyclization was further proved using various 2D NMR experiments (COSY, TOCSY, and ROESY) to examine the crosslinking of the CAAKAAC peptide with BKD-1 to produce **P2** in DMSO-d_6 (Fig. 2e, ESI Section VII and Fig. S5, S6†). The ROESY experiment elicited significant inter-residue

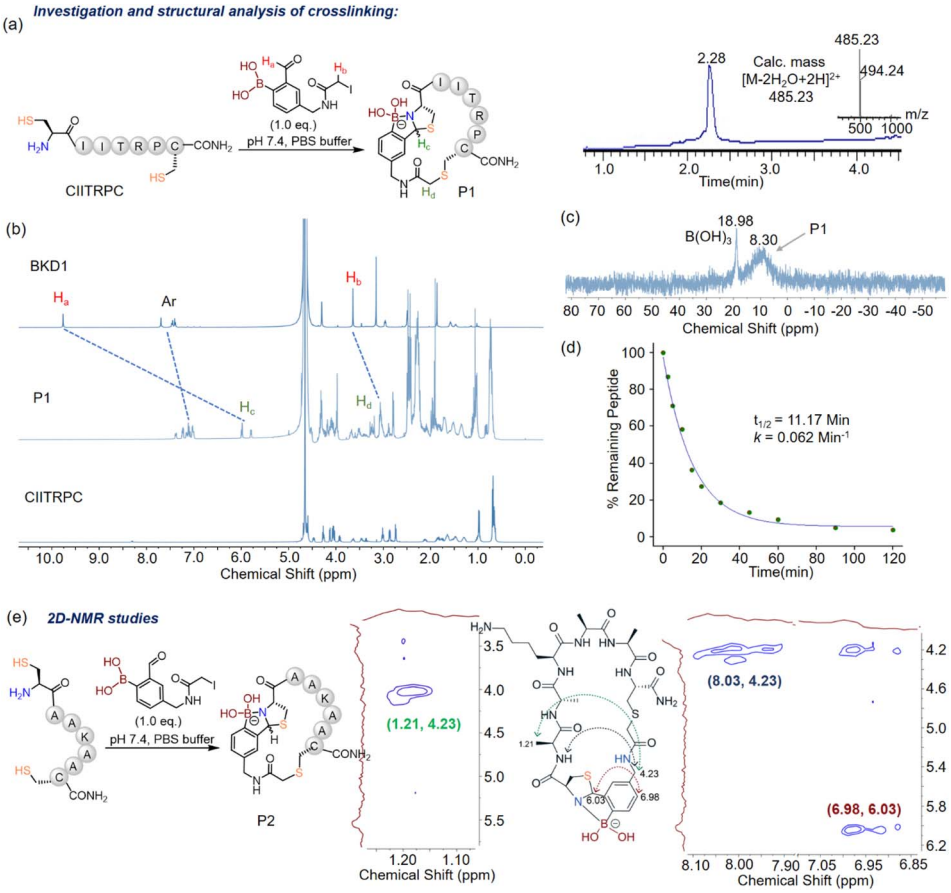

Fig. 2 (a) Scheme of the peptide crosslinking with BKD1 resulting in the macrocyclization of the model peptide CIITRPC. The LC-MS profile of the reaction mixture containing CIITRPC and **BKD1** (1 : 1) shows the expected product as the major component. (b) Investigation of crosslinking of the model peptide using ^{1}H-NMR in (1 : 4) D_2O : PBS (7.4). Three major changes in the ^{1}H-NMR chemical shifts of the peaks of BKD1 (*viz.* formyl, aromatic, and methylene iodide) demonstrate the regioselective crosslinking. (c) ^{11}B-NMR spectrum of **P1**, which clearly establishes the N–B connection in the azaborolo thiazolidine (ABT) graft. (d) Reaction kinetics of crosslinking at pH 7.4 monitored through LC-MS over time by quenching with 1 M HCl (for details, see ESI Section VI†); the peak area of the leftover CIITRPC in the reaction mixture at certain time intervals was calculated to monitor the reaction progress. (e) Assigned NOEs in the ROESY spectra, demonstrating the regioselective crosslinking in **P2**. The colored arrows in the **P2** chemical structure represent the primary NOEs observed, which correlate with 2D-NMR data shown in brackets.

cross-peaks, such as Ala–CH_3–β(H) ↔ Benz–CH_2 (strong), Ala–NH ↔ Benz–CH_2 (medium), **ABT**–C–H ↔ Ar–H and **ABT**–C–H ↔ Benz–CH_2 (medium), supporting the presence of a stable macrocyclic structure in the BKD-1 crosslinked peptide (Fig. 2e). Additionally, clean conversions were observed within the range of 1 mM substrate concentration (ESI Section IX and Fig. S8†), whereas higher probe concentrations (>1 mM) led to a loss in reaction orthogonality on the cysteine centers.

Substrate scope for monocyclization and bicyclization

The scope of this novel crosslinking methodology with BKD-1 was explored with various biologically active peptide sequences (RGD (shortest) and gomesin (largest)). Most peptides showed >90% regioselective crosslinked product conversion in PBS (pH 7.4) within 60 min, independent of the length and amino acid sequences (Fig. 3a), as was evident from the recorded HPLC, mass (ESI Section X and Fig. S9–S14†) and ^{1}H-NMR data (ESI Section XI and Fig. S15–S17†). The crosslinked thiazolidine diastereomers did not separate in the routinely used HPLC gradient, but in some cases, a hump or a broad peak was observed near the crosslinked peptide peak due to the protonation of the N-atom in the ABT motif in acidic HPLC buffer. All peptides were isolated through HPLC purifications with a good yield (Fig. 3a). Notably, this crosslinking could be executed at a low micromolar concentration of BKD1 in a quantitative manner due to a selective, rapid, and highly productive association between 2-FPBA and N-terminal cysteine,[48] based on the advantage of the designed lynchpin, which avoids the side reactions of using the over-alkylating (iodoacetamide) agent.[49]

A second disulfide ring could also be appended to the crosslinked ABT peptides *via* strategic combination with the iodine-mediated disulfide crosslinking of Acm-protected cysteine pairs.[50] Towards this end, native peptides containing an additional pair of Acm-protected cysteines, *viz.* those derived from conotoxin and gomensin (Fig. 3b), were first subjected to BKD-1 coupling, resulting in rapid crosslinking between the free N-terminus and a backbone cysteine to produce Cono-Cy

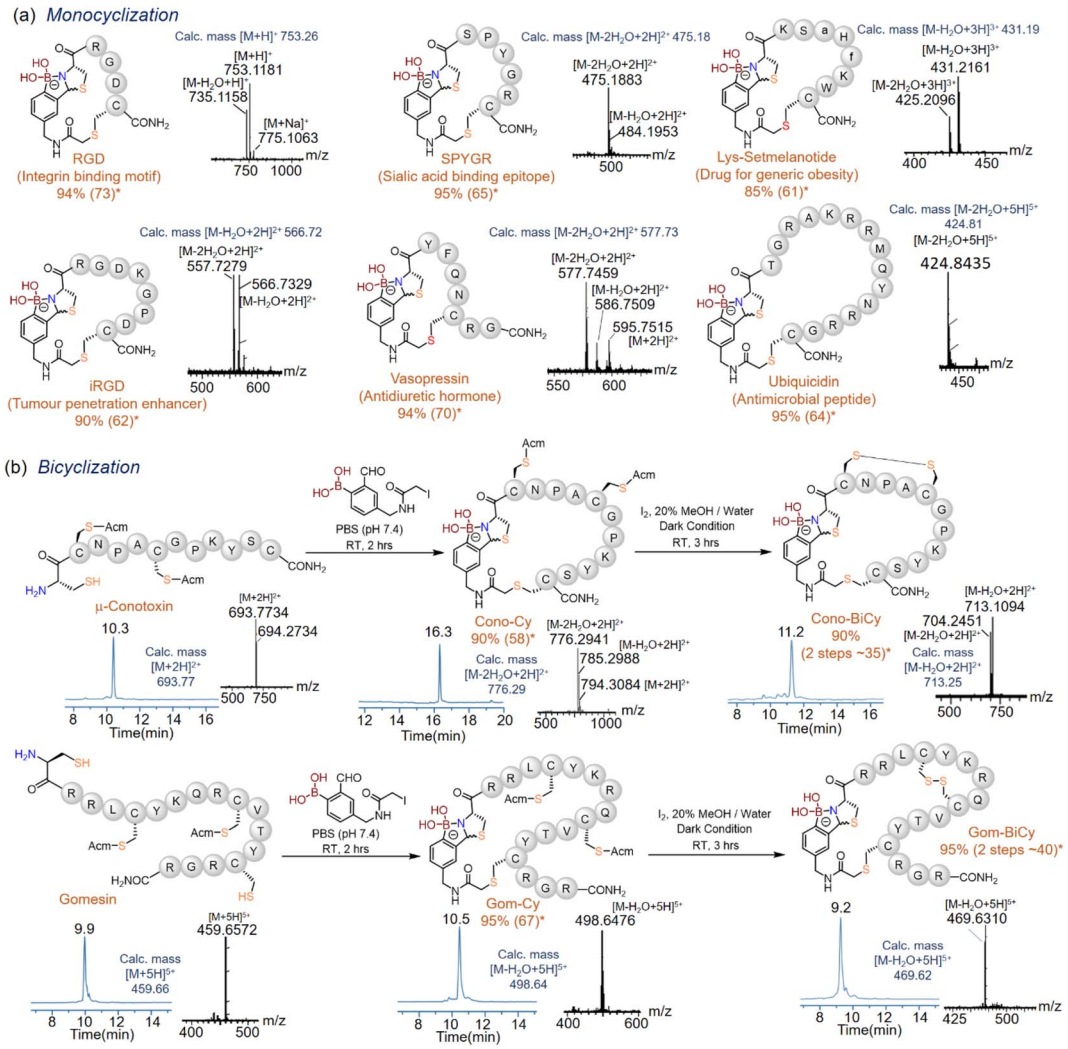

Fig. 3 (a) Demonstration of the regioselective crosslinking strategy using various biologically active peptide sequences. (b) Stepwise demonstration of regioselective bicyclisation strategy for conotoxin and gomesin sequences. Purified HPLC data for linear and monocyclized peptides (conotoxin and gomesin) are shown. HPLC data of crude reaction mixtures for the final step, which clearly depict the quantitative conversion, and the associated mass data confirming the crosslinked products. Monoisotopic mass data are shown for better illustration. Conversion of the crude reaction was analyzed using LC at 220 nm by estimating the peak area of the unreacted linear peptide and is represented with %, and the isolated yields are shown in parentheses ()*.

and Gom-Cy in near-quantitative conversions. The latter, upon iodine-mediated regioselective disulfide bridging between the Acm-protected cysteine pairs, then appended the second ring[34] to furnish the bicyclic peptides Cono-BiCy and Gom-BiCy, respectively (ESI Section XII and Fig. S18, S19†). This simplified approach for regioselective bicyclization in solution-phase peptide chemistry holds great promise for the synthesis of bioactive bicyclic peptides with an enhanced chemical space and desirable biological properties.[51]

Stability and reversibility of crosslinked peptides

Due to the labile nature of the thiazolidine ring at acidic pH values,[47] the solution stability of the cyclic ABT peptides was also investigated, *e.g.*, with **P1** *via* ^{1}H-NMR (Fig. 4a). The cyclic peptide **P1** was found to be stable in a PBS buffer (pH = 7.4) over 15 days, as shown in the LC traces beyond that time (ESI Section XIV and Fig. S21†). With lowering of the pH, slight downfield shifts and broadening of the aromatic protons and thiazolidine ring were observed, perhaps due to dynamic protonation and deprotonation of the N-atom in the ABT graft in acidic media (Fig. 4a, ESI Section XIII†). However, complete dissociation of the thiazolidine ring with the appearance of an aldehyde peak corresponding to the 2-FPBA moiety was never observed, demonstrating the high stability of **P1** under a wide range of pH values. Contrary to the rapid oxidation of phenylboronic acid by H_2O_2 under physiological conditions,[52] cyclic peptide **P1** showed remarkable stability in ~150 μM H_2O_2 even after 6 h (Fig. 4c, ESI Section XV†) due to strong coordination between N and B atoms in the ABT motif. A maximum concentration of ~100 μM can be found in the case of malignant tumor cells,[53] and ABT-crosslinked peptide showed notable compatibility in the most abundant reactive oxygen species (ROS) environment.

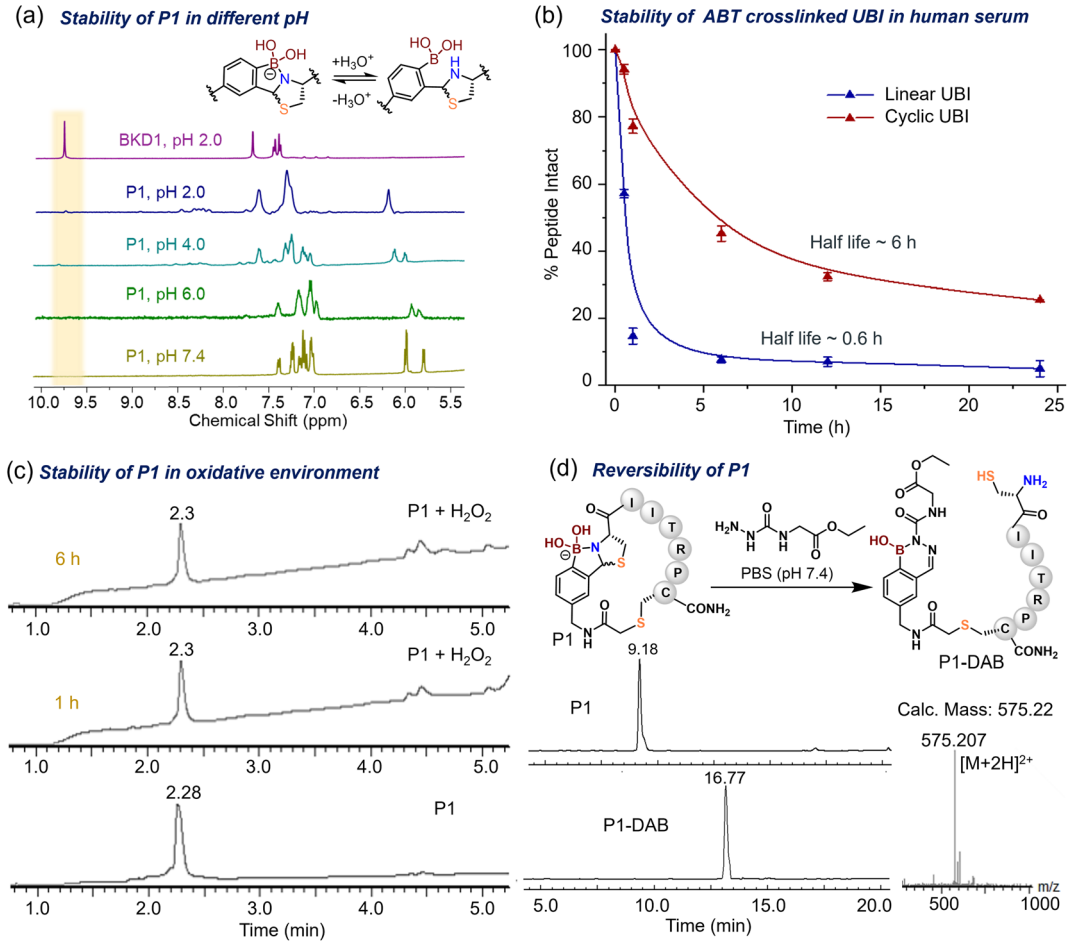

Fig. 4 Stability studies of crosslinked peptides. (a) ^{1}H-NMR profile of P1 at different pH values. The aromatic region is shown for better resolution and compared with the BKD1 profile. (b) Serum (~20% in PBS 7.4) stability of ABT-crosslinked ubiquicidine (UBI 29–41) peptide compared with that of the linear UBI 29–41 peptide. The crosslinked UBI showed a 10-fold increase in stability. (c) LC-MS profile of P1 (~100 μM) treated with ~150 μM hydrogen peroxide in PBS (pH 7.4) for up to 6 h, demonstrating its stability (Method 1 Section Ic in ESI†). (d) Linearization of P1 investigated using HPLC and mass in the presence of ~100 μM semicarbazide derivative in PBS (pH 7.4) for 20 min (Method 3 Section Ic in ESI†).

Interestingly, we found that ABT-crosslinked ubiquicidine (UBI 29–41, Fig. 3a) peptide exhibited a half-life 10 times that of the linear precursor in human serum (~20% diluted in PBS, Fig. 4b). UBI, an antimicrobial peptide, was modified with N- and C-terminus Cys for ABT crosslinking. The Cys residues of the linear analog (linear UBI) were alkylated with iodoacetamide to restrict oxidative cyclization in the physiological buffer system.

Interestingly, the ABT peptide **P1** could be linearized with an equimolar amount of the biocompatible nucleophile semicarbazide[54] in PBS (7.4) due to the formation of a highly stable diazaborine conjugate, as confirmed using LC-MS. The peptide (**P1**) linearization *via* diazaborine formation was further confirmed using ^{1}H-NMR after treatment with phenylhydrazine (ESI Section XVI and Fig. S23†), demonstrating that this crosslinking strategy responds to certain chemical stimuli such as semicarbazide and hydrazine. However, the ABT unit appeared to be stable against exchange from free cysteine, as demonstrated by time-dependent NMR analysis of the reaction between **P1** (~1 mM) and free cysteine (~5 mM) in (1 : 4) D_2O : PBS (7.4) for 10 hours (ESI Section XVII and Fig. S24†). The above studies clearly demonstrated that the ABT-crosslinked peptides show high chemical stability against endogenous stimuli such as acidic pH, ROS, and cysteamine-group-containing molecules.

Crosslinking for folding and intracellular delivery

To augment the significance of the boronic acid lynchpin, we postulated that the method would permit the spontaneous folding of a biologically active peptide into a favorable secondary structure. Further, to facilitate the intracellular delivery of the peptide, the boronic acid moiety can be used to conjugate a drug that is reported to selectively bind to cell surface receptors. In order to investigate the proposal, KLA peptide[55,56] was remodeled *in silico* (ESI Section XVIII†) with appropriate spacers and cysteine, which was expected to enhance the total helical content upon ABT crosslinking (Fig. 5a). The KLA peptide is derived from melittin and exhibits

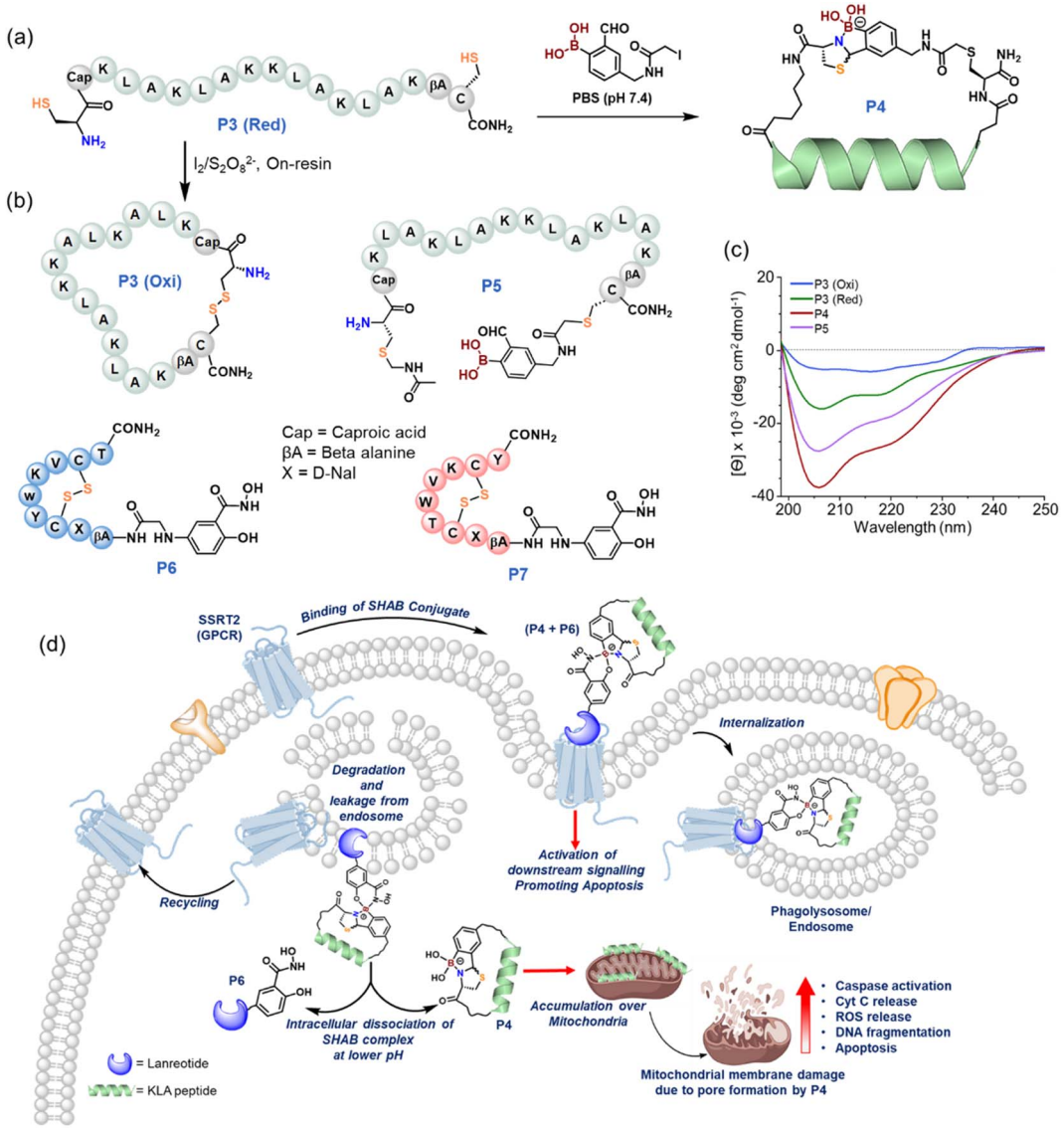

Fig. 5 (a) Reaction scheme of the regioselective crosslinking of linear KLA peptide (**P3 Red**) to yield ABT-crosslinked KLA (**P4**) and disulfide-crosslinked KLA (**P3 Oxi**). (b) Chemical structure of 2-FPBA conjugated linear KLA (**P5**), salicylhydroxamic acid (SHA) conjugated lanreotide (binds to SSR2) and scrambled lanreotide (does not bind to SSR2). (c) CD spectra of **P3**–**P5**, comparing the content of helicity and impact of ABT macrocyclization, recorded in TFE : PBS (7.4) (1 : 1) at peptide concentrations of 50 μM. (d) Scheme representing the delivery of **P4** peptide *via* the formation of a thermodynamically stable salicylhydroxamic boronate (SHAB) conjugate with SSR2-specific **P6** peptide and controlled release of **P4** in endosomes at lower pH to act on mitochondria membrane lysis.

a strong affinity for negatively charged phospholipid membranes.[55,56] Its helical conformation induces pore formation on the surfaces of mitochondrial membranes. Consequently, the release of cytochrome-c into the cytosol is triggered, activating apoptotic or necrotic cell death pathways,[57–59] highlighting its potency in combating cancer. Towards this end, the designed KLA linear precursor (**P3** (**Red**)) was crosslinked with BKD1 to yield **P4** (ESI Section XIX and Fig. S27†) and oxidized to prepare a disulfide-crosslinked KLA control (**P3** (**Oxi**)). Circular dichroism (CD) analyses illustrated a >5-fold enhancement of helical content in KLA upon ABT crosslinking (**P4**) compared to **P3** (**Oxi**) (Fig. 5c, ESI Section XX†), which is in agreement with computational estimations (Fig. S25†). In a control CD experiment, an *S*-alkylated linear KLA (**P5**) peptide having a 2-FPBA moiety (Fig. 5b) demonstrated a ∼3.6-fold increase in peptide folding compared to **P3** (**Oxi**). We believe that the spontaneous and random cyclization *via* iminoboronate formation[60] between 2-FPBA and the lysine side chains in **P5** resulted in these improvements in helicity, which verifies that the appropriate crosslinking of the KLA peptide is essential for better helical folding. Overall, the strategic ABT crosslinking of KLA peptide enabled helical folding to be induced to a greater extent.

We further sought to explore whether **P4** (ABT-crosslinked) exhibits better apoptotic activity than **P5** (linear). Notably, the endocytosis of KLA peptide is limited to eukaryotic cells,[61–63] and the cellular entry can be enhanced by conjugating KLA with targeting motifs such as hyaluronic acid[64,65] or polyarginine.[65] However, our methodology could address this limitation *via* the

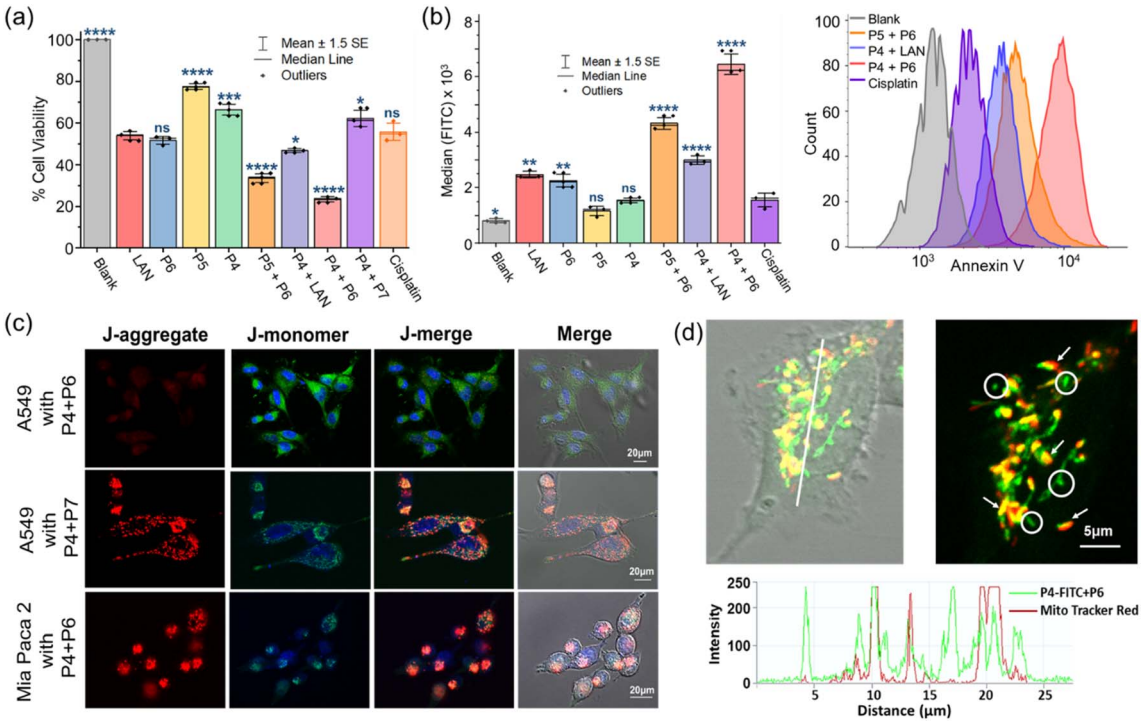

Fig. 6 Antiproliferative activity studies of individual peptides (lanreotide (LAN), **P4**–**P6**) and SHAB conjugates with **P4**, **P6**, and **P7** demonstrating the effectiveness of combined therapy. (a) MTT assay and (b) flow cytometry quantitative assay. All data are triplicated, and studies were repeated twice ($n = 2$) to check their reproducibility. The fluorescence intensity presented in the bar graph is subtracted from the autofluorescence intensity associated with non-treated and non-stained cells. Results are represented as the mean of 6 readings ± SD. Statistical analysis was performed using Graph Pad Prism 4 software and a two-way ANOVA test. Statistical significance for p-values is < 0.05: *P < 0.05, **P < 0.01, ***P < 0.001, ****P < 0.001. (c) LSCM images for JC-1 assay: A549 and Mia PaCa-2 were treated with **P4** in combination with lanreotide and scrambled lanreotide to demonstrate the mechanism of action for **P4** apoptotic activity. J-aggregate (red channel), J-monomer (merged FITC and DAPI), J-merge (red, FITC, and DAPI combined), and merge (white light merged with all channels) show the evident activity of **P4** in causing mitochondrial damage. (d) Fluorescence signals of Mitotracker (red) and P4-FITC (green) are merged to understand the selectivity of **P4** toward mitochondria, and the circled clusters with only green fluorescence are perhaps phagolysosomes *via* which **P4** was delivered into the cells. Fluorescence signals at the white line clearly depict the overlapped (red + FITC) and green-only (FITC) intensities.

appended boronic acid moiety in crosslinked KLA (**P4**). We postulated that a somatostatin peptide analog functionalized with the salicylhydroxamic (SHA) moiety could readily conjugate with the crosslinked KLA peptide (**P4**) *via* salicylhydroxamic boronate (SHAB) formation, and that the combined formulate could selectively bind to the overexpressed somatostatin receptor in cancer cells, similar to an antibody–drug conjugate. Further, the conjugate would be endocytosed to release **P4**, triggered by the lower pH in cytosol, which would subsequently induce apoptosis (Fig. 5d). In addition, the combined antiproliferative activity of the somatostatin analog and crosslinked KLA could represent a better approach to combating cancer.[66] In order to test this hypothesis, lanreotide (LAN),[67] a synthetic analog of somatostatin that binds to SSR2 selectively, was engineered with an SHA moiety at the N-terminus (**P6**, Fig. 5b, ESI Section XXI and Fig. S28†). A scrambled LAN peptide adjoined to SHA (**P7**) and **P5** was considered as controls. The formation of SHAB conjugates between **P4** and **P6** was confirmed using mass spectrometry (ESI Section XXIII and Fig. S29†) before assessing its antiproliferative activity.

Moving forward, we performed MTT assays on the A549 cell line to evaluate our hypothesis of combined therapy. Individual peptides (**P4–6**, ∼20 μM) and three combinations (**P4** + **P6**, **P5** + **P6**, and **P4** + **P7**) prepared by mixing equimolar amounts of each (∼20 μM in culture media) were used in this study. Cisplatin (∼50 μM) and LAN (∼20 μM) were included as positive controls (ESI Section XXIV and Fig. S30a†). After a 12 hour incubation period, we observed that the combination of **P4** + **P6** exhibited the highest cytotoxicity (∼24% cell viability), which is >2-fold higher than that of the individual peptides (Fig. 6a). Although **P4** and **P5** are both anticipated to cross the extracellular membrane with the assistance of **P6** *via* SHAB conjugation, **P5** + **P6** showed a slightly reduced cytotoxic response compared to **P4** + **P6** (∼34% *vs.* ∼24% cell viability), perhaps due to the lower helical content and lower enzymatic stability of **P5** than **P4**. As expected, the individual treatment of A549 with **P5** or **P4** exhibited the least cytotoxicity owing to their poor cell permeability. **P4** provided better results than **P5** to some extent; it probably existed in a compact ABT-crosslinked structure. When **P4** was combined with scrambled LAN (**P7**), the cell apoptosis was compromised ∼2.5-fold compared to that of (**P4** + **P6**), proving the SSR2-assisted delivery of **P4** (Fig. 6a). The SSR2-mediated delivery was further justified the very low antiproliferative activity of **P4** + **P6** in cell lines lacking SSR2

receptors, such as Mia PaCa-2 (Fig. S30b†). The data unambiguously demonstrate the importance of the suitable crosslinking of KLA and the conjugation of KLA with suitable receptor-targeting peptides to create an effective biological response. Further, the control experiment of combined **P4** + LAN treatment exhibited a greatly reduced response (~47% cell viability) compared to the two combinations of **P4** + **P6** and **P5** + **P6**, unambiguously demonstrating the importance of boronic-acid-mediated SHAB conjugation in intracellular peptide delivery. The selective apoptotic activity of **P4** + **P6** in normal cells (HEK329) and cancer cells (A549) was compared, demonstrating that the conceptualized combination therapy is ~2.5-fold more selective toward cancer cells (Fig. S30b†).

We were keen to quantitatively assess the apoptotic activity of combined therapy events to strengthen our hypothesis. Cell apoptosis was monitored in flow cytometry by labeling externalized phosphatidylserine with annexin V-FITC (ESI Section XXV and Fig. S31†). The fluorescence readout (Fig. 6b) demonstrated a consistent outcome ascribed to the MTT assay, in which **P4** + **P6** combinedly displayed ~1.45 and ~2.1-fold higher fluorescence median value intensities than the apoptotic activity of **P5** + **P6** and **P4** + **LAN**, respectively. Notably, the SHAB conjugate (**P4** + **P6**) showed >2.5-fold higher antiproliferative activity compared to any individual component. Together, these findings validate the potential of combination therapy, demonstrate successful intracellular delivery, and highlight the uniqueness of this crosslinking strategy.

Mechanism of action

We set out to reinvestigate the mechanism of action of the apoptotic activity shown by **P4**. KLA peptides are known to damage mitochondrial membranes, which results in depolarization of the mitochondrial membrane with a drop in potential ($\Delta\psi_m$).[68] This work examined the mitochondria-regulated apoptosis pathway using fluorescence probe JC-1 under a laser scanning confocal microscope (LSCM). It has been reported that the green monomer of JC-1 enters the cytoplasm and forms red fluorescent aggregates in normal mitochondria, namely red J-aggregates, which revert to the monomer stage (green) upon depolarization of the mitochondrial membranes.[69] In view of this mechanism, we noticed the disappearance of red fluorescence (normal mitochondria) and an increase in green fluorescence (monomer in the cytoplasm) in A549 cells when incubated with **P4** + **P6** under LSCM (Fig. 6c, top row). This phenomenon could only be ascribed to serious damage of the mitochondrial membrane of A549 cells by **P4** *via* SSR2-mediated entry, leading to a relatively low $\Delta\psi_m$. In contrast, there is no obvious change in $\Delta\psi_m$ for Mia Paca 2 cells due to the lack of SSRT2-mediated entry of **P4** (Fig. 6c, bottom row). A similar status of A549 was detected for treatment with **P4** + **P7** (Fig. 6c, middle row), indicating that the LAN sequence is essential for SSRT2-mediated cellular entry. In the case of normal epithelial cell line HEK293, a small amount of **P4** + **P6** entry was revealed, because normal cells also express the SSRT2 receptor, but not to the extent of cancerous cells (Fig. S32†); these results were consistent with those of the MTT assays. We noticed that treatment of A549 with **P4** alone damaged neither the plasma membrane nor the mitochondrial membrane under LSCM (Fig. S32†). Finally, treatment with FITC-labeled **P4** (**P4**-FITC, Fig. S26†) for 4 hours, followed by Mito Tracker red, revealed the overlapped regions of green and red fluorescence under LSCM, thus unambiguously demonstrating the **P4** selectivity toward mitochondria (Fig. 6d, shown by arrows). We assumed that the green aggregates (Fig. 6d, indicated by circles) that do not overlap with the Mito Tracker are phagolysosomes that slowly released **P4** to reach the mitochondria. The fluorescence signals (Fig. 6d, bottom intensity graph) that are grounded on the white line perhaps indicate such phenomena.

Conclusion

The report summarizes a new regioselective crosslinking regime, resulting in a new class of borono-cyclopeptides for biochemical exploitation by deploying a bis-electrophilic lynchpin. The designed tandem bis-electrophile, which is constructed by uniting *ortho* carbonyl phenylboronic acid and iodoacetamide, manifested rapid crosslinking between the N-terminus and backbone cysteine at physiological pH at micromolar concentration. This technology is high-yielding and operationally simple, irrespective of the amino acid residues or chain lengths of the peptides. Interestingly, crosslinked peptides exhibited stability at physiological and acidic pH and under a physiologically significant ROS stimulus (H_2O_2). The crosslinked peptide could be linearized upon suitable applications of hydrazine stimuli by releasing an important diazaborine pharmacophore, which proved the superiority of this crosslinking method. The method clearly achieves regioselective bicyclization, as evidenced by conotoxin and gomesin construction, which could create multiple valuable opportunities in drug discovery platforms. The ABT graft that achieved the cyclopeptide frameworks showed further utility in folding, drug delivery, and combined cancer therapy. We showed that the ABT-graft-induced folded pro-apoptotic peptide could be delivered to mitochondria with the assistance of a somatostatin analog *via* dynamic SHAB chemistry to achieve improved retardation of cancer growth. In a nutshell, our investigation advances two important goals of chemical biology, including providing a solution to the synthetic challenge of late-stage modification of peptide cyclization in therapeutic conditions and expanding the nexus of possibilities of cyclic peptides for modern drug discovery. We speculate that our contribution will pave the way for many directions in peptide therapeutics.

Data availability

The data supporting this article have been included in the ESI.†

Author contributions

AB conceptualized and supervised the project. BKD performed all crosslinking chemistry and analysis with the assistance of SC, BNP, and SD. All biological experiments were performed by AC. NMT helped in computational model design and MD

simulation. The manuscript was written by the contribution of all authors.

Conflicts of interest

There are no conflicts to declare.

Acknowledgements

We gratefully welcome the financial assistance provided by IIT Ropar through the ISIRD grant and the core research grant (CRG/2022/007757) from SERB, India. BKD thanks IIT Ropar for the postdoctoral fellowship. SC and AC express gratitude to IIT Ropar for providing a PhD fellowship. NMT expresses gratitude to DST for giving a fellowship. We also appreciate the IIT Ropar central research facility for the HRMS and NMR facilities and the department LCMS facility (SR/FST/CS-I/2018/55). The IIT Ropar HPC facility was used for all computations. We are grateful to Kashiv Biosciences in India for their assistance.

Notes and references

1 A. Capecchi and J. L. Reymond, *Med. Drug Discovery*, 2021, **9**, 100081.
2 C. Bechtler and C. Lamers, *RSC Med. Chem.*, 2021, **12**, 1325–1351.
3 A. Boto, C. C. González, D. Hernández, I. Romero-Estudillo and C. J. Saavedra, *Org. Chem. Front.*, 2021, **8**, 6720–6759.
4 C. M. B. K. Kourra and N. Cramer, *Chem. Sci.*, 2016, **7**, 7007–7012.
5 S. Lindman, G. Lindeberg, P.-A. Frändberg, F. Nyberg, A. Karlén and A. Hallberg, *Bioorg. Med. Chem.*, 2003, **11**, 2947–2954.
6 M. Ueki, T. Ikeo, K. Hokari, K. Nakamura, A. Saeki and H. Komatsu, *Bull. Chem. Soc. Jpn.*, 1999, **72**, 829–838.
7 L. R. Malins, J. N. deGruyter, K. J. Robbins, P. M. Scola, M. D. Eastgate, M. R. Ghadiri and P. S. Baran, *J. Am. Chem. Soc.*, 2017, **139**, 5233–5241.
8 B. Li, Z. Wan, H. Zheng, S. Cai, H.-W. Tian, H. Tang, X. Chu, G. He, D.-S. Guo, X.-S. Xue and G. Chen, *J. Am. Chem. Soc.*, 2022, **144**, 10080–10090.
9 Y. Goto, A. Ohta, Y. Sako, Y. Yamagishi, H. Murakami and H. Suga, *ACS Chem. Biol.*, 2008, **3**, 120–129.
10 N. Bionda, A. L. Cryan and R. Fasan, *ACS Chem. Biol.*, 2014, **9**, 2008–2013.
11 W. S. Horne, C. A. Olsen, J. M. Beierle, A. Montero and M. R. Ghadiri, *Angew. Chem., Int. Ed.*, 2009, **48**, 4718–4724.
12 M. G. Wuo, A. B. Mahon and P. S. Arora, *J. Am. Chem. Soc.*, 2015, **137**, 11618–11621.
13 Y.-W. Kim, T. N. Grossmann and G. L. Verdine, *Nat. Protoc.*, 2011, **6**, 761–771.
14 H. E. Blackwell, J. D. Sadowsky, R. J. Howard, J. N. Sampson, J. A. Chao, W. E. Steinmetz, D. J. O'Leary and R. H. Grubbs, *J. Org. Chem.*, 2001, **66**, 5291–5302.
15 T. Fukuzumi, L. Ju and J. W. Bode, *Org. Biomol. Chem.*, 2012, **10**, 5837–5844.
16 J. W. Bode, R. M. Fox and K. D. Baucom, *Angew. Chem., Int. Ed.*, 2006, **45**, 1248–1252.
17 H. C. Hayes, L. Y. P. Luk and Y. H. Tsai, *Org. Biomol. Chem.*, 2021, **19**, 3983–4001.
18 P. Yang, M. J. Širvinskas, B. Li, N. W. Heller, H. Rong, G. He, A. K. Yudin and G. Chen, *J. Am. Chem. Soc.*, 2023, **145**, 13968–13978.
19 C. Bechtler and C. Lamers, *RSC Med. Chem.*, 2021, **12**, 1325–1351.
20 S. Laps, F. Atamleh, G. Kamnesky, S. Uzi, M. M. Meijler and A. Brik, *Angew. Chem., Int. Ed.*, 2021, **60**, 24137–24143.
21 S. Laps, F. Atamleh, G. Kamnesky, H. Sun and A. Brik, *Nat. Commun.*, 2021, **12**, 870.
22 M. J. S. A. Silva, H. Faustino, J. A. S. Coelho, M. V Pinto, A. Fernandes, I. Compañón, F. Corzana, G. Gasser and P. M. P. Gois, *Angew. Chem., Int. Ed.*, 2021, **60**, 10850–10857.
23 T. R. Oppewal, I. D. Jansen, J. Hekelaar and C. Mayer, *J. Am. Chem. Soc.*, 2022, **144**, 3644–3652.
24 Y. Wu, C. Li, S. Fan, Y. Zhao and Y. Zhao, *Bioconjugate Chem.*, 2021, **32**, 2065–2072.
25 X. Zheng, Z. Li, W. Gao, X. Meng, X. Li, L. Y. P. Luk, Y. Zhao, Y. H. Tsai and C. Wu, *J. Am. Chem. Soc.*, 2020, **142**, 5097–5103.
26 J. T. Hampton, T. J. Lalonde, J. M. Tharp, Y. Kurra, Y. R. Alugubelli, C. M. Roundy, G. L. Hamer, S. Xu and W. R. Liu, *ACS Chem. Biol.*, 2022, **17**, 2911–2922.
27 R. Wills, V. Adebomi and M. Raj, *ChemBioChem*, 2021, **22**, 52–62.
28 I. V. Smolyar, A. K. Yudin and V. G. Nenajdenko, *Chem. Rev.*, 2019, **119**, 10032–10240.
29 B. J. Wang and M. P. Groziak, *Adv. Heterocycl. Chem.*, 2016, **118**, 47–90.
30 B. C. Das, M. Adil Shareef, S. Das, N. K. Nandwana, Y. Das, M. Saito and L. M. Weiss, *Bioorg. Med. Chem.*, 2022, **63**, 116748.
31 N. A. Schilling, A. Berscheid, J. Schumacher, J. S. Saur, M. C. Konnerth, S. N. Wirtz, J. M. Beltrán-Beleña, A. Zipperer, B. Krismer, A. Peschel, H. Kalbacher, H. Brötz-Oesterhelt, C. Steinem and S. Grond, *Angew. Chem., Int. Ed.*, 2019, **58**, 9234–9238.
32 S. Chatterjee and A. Bandyopadhyay, *Org. Lett.*, 2023, **25**, 2223–2227.
33 J. B. Mitra, S. Chatterjee, A. Kumar, A. Bandyopadhyay and A. Mukherjee, *RSC Med. Chem.*, 2022, **13**, 1239–1245.
34 S. Chatterjee, A. Chowdhury, S. Saproo, N. Mani Tripathi, S. Naidu and A. Bandyopadhyay, *Chem.–Eur. J.*, 2023, e202303327.
35 D. Li, Y. Chen and Z. Liu, *Chem. Soc. Rev.*, 2015, **44**, 8097–8123.
36 G. Wulff, M. Lauer and H. Böhnke, *Angew Chem. Int. Ed. Engl.*, 1984, **23**, 741–742.
37 N. Sahiba, A. Sethiya, J. Soni, D. K. Agarwal and S. Agarwal, *Top. Curr. Chem.*, 2020, **378**, 34.
38 S. Huh, N. Batistatou, J. Wang, G. J. Saunders, J. A. Kritzer and A. K. Yudin, *RSC Chem. Biol.*, 2024, **5**, 328–334.
39 G. A. Ellis, M. J. Palte and R. T. Raines, *J. Am. Chem. Soc.*, 2012, **134**, 3631–3634.

40 S. Chatterjee, N. M. Tripathi and A. Bandyopadhyay, *Chem. Commun.*, 2021, **57**, 13629–13640.
41 S. Sinha, P. Gaur, S. Dev, S. Mukhopadhyay, T. Mukherjee and S. Ghosh, *Sens. Actuators, B*, 2015, **221**, 418–426.
42 S. Chatterjee, E. V. Anslyn and A. Bandyopadhyay, *Chem. Sci.*, 2021, **12**, 1585–1599.
43 K. Li, W. Wang and J. Gao, *Angew. Chem., Int. Ed.*, 2020, **59**, 14246–14250.
44 H. Choi, M. Kim, J. Jang and S. Hong, *Angew. Chem., Int. Ed.*, 2020, **59**, 22514–22522.
45 F.-J. Chen and J. Gao, *Chem.–Eur. J.*, 2022, **28**, e202201843.
46 C. P. Ramil, P. An, Z. Yu and Q. Lin, *J. Am. Chem. Soc.*, 2016, **138**, 5499–5502.
47 A. Bandyopadhyay, S. Cambray and J. Gao, *Chem. Sci.*, 2016, **7**, 4589–4593.
48 N. C. Rose, A. V. Sanchez, E. F. Tipple, J. M. Lynam and C. D. Spicer, *Chem. Sci.*, 2022, **13**, 12791–12798.
49 P. G. Hains and P. J. Robinson, *J. Proteome Res.*, 2017, **16**, 3443–3447.
50 R. J. Spears, C. McMahon and V. Chudasama, *Chem. Soc. Rev.*, 2021, **50**, 11098–11155.
51 F.-J. Chen, N. Pinnette, F. Yang and J. Gao, *Angew. Chem., Int. Ed.*, 2023, e202306813.
52 A. Chowdhury, S. Chatterjee, A. Kushwaha, S. Nanda, T. J. Dhilip Kumar and A. Bandyopadhyay, *Chem.–Eur. J.*, 2023, e202300393.
53 B. Halliwell, M. V. Clement and L. H. Long, *FEBS Lett.*, 2000, **486**, 10–13.
54 A. Bandyopadhyay, S. Cambray and J. Gao, *J. Am. Chem. Soc.*, 2017, **139**, 871–878.
55 H. M. Ellerby, W. Arap, L. M. Ellerby, R. Kain, R. Andrusiak, G. Del Rio, S. Krajewski, C. R. Lombardo, R. Rao, E. Ruoslahti, D. E. Bredesen and R. Pasqualini, *Nat. Med.*, 1999, **5**, 1032–1038.
56 L. Agemy, D. Friedmann-Morvinski, V. R. Kotamraju, L. Roth, K. N. Sugahara, O. M. Girard, R. F. Mattrey, I. M. Verma and E. Ruoslahti, *Proc. Natl. Acad. Sci. U. S. A.*, 2011, **108**, 17450–17455.
57 A. Tossi, L. Sandri and A. Giangaspero, *Pept. Sci.*, 2000, **55**, 4–30.
58 S. Hyun, S. Lee, S. Kim, S. Jang, J. Yu and Y. Lee, *Biomacromolecules*, 2014, **15**, 3746–3752.
59 J. Li, K. Hu, H. Chen, Y. Wu, L. Chen, F. Yin, Y. Tian and Z. Li, *Chem. Commun.*, 2017, **53**, 10452–10455.
60 A. Bandyopadhyay and J. Gao, *J. Am. Chem. Soc.*, 2016, **138**, 2098–2101.
61 T. Utsugi, A. J. Schroit, J. Connor, C. D. Bucana and I. J. Fidler, *Cancer Res.*, 1991, **51**, 3062–3066.
62 I. D. Alves, M. Carré, M.-P. Montero, S. Castano, S. Lecomte, R. Marquant, P. Lecorché, F. Burlina, C. Schatz, S. Sagan, G. Chassaing, D. Braguer and S. Lavielle, *Biochim. Biophys. Acta, Biomembr.*, 2014, **1838**, 2087–2098.
63 J. Connor, C. Bucana, I. J. Fidler and A. J. Schroit, *Proc. Natl. Acad. Sci. U. S. A.*, 1989, **86**, 3184–3188.
64 J. Lee, E.-T. Oh, H. Lee, J. Kim, H. G. Kim, H. J. Park and C. Kim, *Bioconjugate Chem.*, 2020, **31**, 43–50.
65 J. Lee, E.-T. Oh, Y. Joo, H. G. Kim, H. J. Park and C. Kim, *New J. Chem.*, 2020, **44**, 19734–19741.
66 R. B. Mokhtari, T. S. Homayouni, N. Baluch, E. Morgatskaya, S. Kumar, B. Das and H. Yeger, *Oncotarget*, 2017, **8**, 38022–38043.
67 M. Michael, R. Garcia-Carbonero, M. M. Weber, C. Lombard-Bohas, C. Toumpanakis and R. J. Hicks, *Oncologist*, 2017, **22**, 272–285.
68 W. H. Chen, X. D. Xu, G. F. Luo, H. Z. Jia, Q. Lei, S. X. Cheng, R. X. Zhuo and X. Z. Zhang, *Sci. Rep.*, 2013, **3**, 1–7.
69 B. K. Wagner, T. Kitami, T. J. Gilbert, D. Peck, A. Ramanathan, S. L. Schreiber, T. R. Golub and V. K. Mootha, *Nat. Biotechnol.*, 2008, **26**, 343–351.